Available online at www.sciencedirect.com
ScienceDirect
Acta Materialia 56 (2008) 809–820
Acta MATERIALIA
www.elsevier.com/locate/actamat

Influence of stacking-fault energy on microstructural characteristics of ultrafine-grain copper and copper–zinc alloys

Levente Balogh [a], Tamás Ungár [a], Yonghao Zhao [b], Y.T. Zhu [c], Zenji Horita [d], Cheng Xu [e], Terence G. Langdon [e,f,*]

[a] Department of Materials Physics, Eötvös University, Budapest, P.O. Box 32, H-1518, Hungary
[b] Department of Chemical Engineering and Materials Science, University of California, Davis, CA 95616, USA
[c] Materials Physics and Applications Division, MS G755, Los Alamos National Laboratory, Los Alamos, NM 87545, USA
[d] Department of Materials Science and Engineering, Faculty of Engineering, Kyushu University, Fukuoka 819-0395, Japan
[e] Departments of Aerospace & Mechanical Engineering and Materials Science, University of Southern California, Los Angeles, CA 90089-1453, USA
[f] Materials Research Group, School of Engineering Sciences, University of Southampton, Southampton SO17 1BJ, UK

Received 23 July 2007; received in revised form 17 October 2007; accepted 17 October 2007

Abstract

Experiments were conducted on samples of pure Cu and two Cu–Zn alloys to evaluate the influence of the stacking-fault energy (SFE) on microstructural development when processing using high-pressure torsion (HPT). Transmission electron microscopy, X-ray diffraction and hardness measurements were used for microstructural evaluation and the results show consistency between these techniques. Grain sizes in the nanometer range were formed at the edges of the HPT disks, larger submicrometer grains were formed in the disk centers and the measured grain sizes decreased with decreasing SFE. There was negligible twinning in pure Cu but the densities of dislocations and twins increased with increasing Zn content and thus with decreasing SFE. The values of the Vickers microhardness were lower in the centers of the disks for the two Cu–Zn alloy and this is consistent with the low SFE and slow rates of recovery.

Keywords: Copper alloys; High-pressure torsion; Severe plastic deformation; Stacking-fault energy; X-ray diffraction

1. Introduction

Processing through the application of severe plastic deformation (SPD) is now accepted as the optimum procedure for producing exceptional grain refinement to the submicrometer or nanometer level [1]. Several different SPD processing techniques are available but most attention has focused to date on equal-channel angular pressing (ECAP) where samples are pressed through a die constrained within a channel that is bent through an abrupt angle [2]. Processing by ECAP has an advantage because it can be scaled-up easily for use with relatively large bulk samples [3] and, in addition, the principles of ECAP may be incorporated into continuous procedures such as rolling [4,5] and the conform process [6]. Nevertheless, the grains produced by ECAP are invariably >100 nm and it is therefore difficult to make use of ECAP for an evaluation of the properties of materials having grain sizes within the nanometer range.

Processing by high-pressure torsion (HPT) represents an alternative SPD procedure [7–9] wherein a sample, in the form of a thin disk, is subjected to a high pressure and concurrent torsional straining using procedures based on the principles first introduced by Bridgman [10]. Although

* Corresponding author. Address: Departments of Aerospace and Mechanical Engineering and Materials Science, University of Southern California, Los Angeles, CA 90089-1453, USA. Tel.: +1 213 740 0491; fax: +1 213 740 8071.
E-mail address: langdon@usc.edu (T.G. Langdon).

1359-6454/$30.00 © 2007 Acta Materialia Inc. Published by Elsevier Ltd. All rights reserved.
doi:10.1016/j.actamat.2007.10.053

processing by HPT is generally restricted to very small samples, there have been recent attempts to extend this approach to larger bulk samples [11]. Furthermore, an important characteristic of HPT is that it generally produces grains which are significantly smaller than those introduced when processing by ECAP [8,12–16].

Many of the investigations of SPD processing conducted to date have concentrated on pure aluminum or aluminum-based alloys where the stacking-fault energies are high, dislocation slip is the primary mode of deformation and grain refinement is achieved through the accumulation of dislocations and subsequent re-arrangement by dynamic recovery. The grain sizes of these materials are invariably within the range of ~200 nm to ~1.5 μm. However, recent investigations have shown that much smaller grain sizes, within the nanometer range, may be achieved in samples of pure Cu and a Cu–Zn alloy where the stacking-fault energies are very low [17] and where twinning becomes an important mode of deformation [18,19].

Since HPT is a heterogeneous mode of deformation, it is reasonable to anticipate the resultant microstructures will be inhomogeneous. Some exploratory microstructural evaluations have been reported to date. Thus, the radial distributions of grain sizes were investigated in Cu processed by HPT using positron annihilation, transmission electron microscopy (TEM) and X-ray diffraction [20,21], and the positron lifetime data indicated an increased free volume in the off-center regions of the deformed disks. Similarly, disks of the $Cu_{60}Zr_{20}Ti_{20}$ alloy were deformed by HPT and investigated for changes in microstructure and phase composition in the radial and thickness directions using X-ray diffraction, scanning calorimetry and microhardness measurements [22,23]. These latter measurements revealed a maximum in hardness at the half-radius position which was related to the finest crystalline phase in the disks.

The present investigation was initiated to critically examine and evaluate the microstructural characteristics in three different copper-based alloys processed by HPT and having a wide range of stacking-fault energies. Specifically, tests were conducted on samples of pure Cu, Cu–10 wt.% Zn and Cu–30 wt.% Zn where the reported stacking-fault energies are ~41, ~22 and ~7 mJ m^{-2}, respectively [24]. These materials were selected because exceptional grain refinement has been demonstrated after HPT processing with measured grain sizes in each material of <100 nm [25,26].

It should be noted that a principal objective of earlier work [25] was to determine grain sizes along the diameters of disks processed by HPT through an evaluation of micrographs recorded using TEM. High-resolution TEM micrographs indicated the presence of twinning in both pure Cu and the two Cu–Zn alloys. In the present investigation, a special high-resolution and microdiffraction X-ray technique was applied in order to determine both the density of twin boundaries and the dislocation densities at different positions along the radii of the deformed disks.

2. Experimental materials and procedures

The tests were conducted using copper of 99.9% purity and a Cu–30% Zn alloy received in the form of rods with diameters of 10 mm and a Cu–10% Zn alloy received as a plate with a thickness of 6 mm. For processing by HPT, disks were prepared from the as-received samples with diameters of 10 mm and thicknesses of ~0.8 mm. These disks were processed by HPT using a facility in which each disk is placed in turn between two anvils, a pressure is applied and torsional straining is then achieved by rotation of the lower anvil [27]. All processing was conducted at room temperature using an imposed pressure of 6 GPa, a rotation speed of 1 rpm and a total of five revolutions.

Following processing by HPT, the samples were examined in three different ways: by TEM, by X-ray diffraction (XRD) and by measuring the Vickers microhardness in the planes of the disks.

For TEM, disks were prepared to a thickness of ~10 μm by mechanical grinding and through the use of diamond-lapping films. Final thinning was achieved for TEM examination using a Gatan Dual Ion Milling System with an Ar^+ accelerating voltage of 4 kV and with liquid nitrogen for cooling of the sample. These specimens were examined in a Philips CM30 microscope operating at 300 kV. Separate images were taken both near the edges of the HPT disks and in the approximate centers of each disk. The grain size distributions were determined by measuring the widths of individual grains along linear traverses.

For XRD, the experimental procedure relied on an earlier report documenting the effect of stacking faults and twinning on the X-ray diffraction patterns [28]. In this report, the DIFFaX code [29] was used to calculate the influence of X-ray line broadening and line shifts through a numerical analysis of ~15,000 subprofiles corresponding to different hkl groups of the first 15 Bragg reflections of face-centered cubic crystals, thereby providing a set of data files that were incorporated into a whole powder pattern fitting procedure designated the convolutional multiple whole-profile (CMWP) fitting program [30]. The present work employed the principles of this approach but made use of an alternative extended CMWP procedure, designated eCMWP, which was described earlier [28]. Using this alternative approach, the eCMWP procedure was applied to determine the twin density, the dislocation structure and the size distribution of grains or subgrains in each disk after HPT processing.

In practice, the X-ray diffraction observations made use of a special high-resolution double-crystal diffractometer having a negligible instrumental effect. This facility involved a fine-focus rotating copper anode and used the symmetrical (220) reflection of a Ge monochronometer. The $K_{\alpha 2}$ component of the Cu radiation was eliminated using a 0.2 mm slit between the X-ray source and the Ge crystal. The cross-section of the beam at the specimen was ~0.1×0.5 mm^2 and the individual profiles were registered using a linear position-sensitive gas flow detector.

The X-ray peaks were located using a fine fluorescent screen located in the position of the specimen to within an accuracy of better than 0.1 mm. This arrangement gave the position of the specimen in the beam during the X-ray operation to an estimated precision of approximately ±0.1 mm. The individual X-ray diffraction patterns were recorded on each specimen in the center, at the half-radius position and near the edge of each HPT disk, where these separate positions are designated the $0R$, $(1/2)R$ and $1R$ positions, respectively, where R is the radius of the disk.

For the microhardness measurements, each disk was mechanically polished, electro-polished to a smooth surface and then measurements were taken using an FM-1e microhardness tester equipped with a Vickers indenter. The procedure adopted for the microhardness measurements was similar to that used in an earlier investigation where hardness measurements were taken on pure aluminum after HPT [31]. Specifically, a series of individual measurements of the Vickers microhardness, H_V, was recorded following a rectilinear grid pattern in which separate measurements were taken over the total area of the disk with individual spacings between each reading of 0.3 mm. This large array of individual measurement points permitted the plotting of color-coded contour maps in which the variations in hardness are represented in visual arrays by changes in color across each cross-sectional area.

3. Experimental results

In an earlier report [25], TEM micrographs corresponding to the outer edge regions of disks deformed similarly by HPT revealed average grain sizes decreasing from 75 to 50 to 10 nm for Cu, Cu–10% Zn and Cu–30% Zn, respectively. The statistical variations in the grain sizes were evaluated by bar diagrams which suggested the presence of log-normal size distributions. In the present report, the differences and similarities of the microstructures in the centers and edge regions of the disks are demonstrated directly by showing TEM micrographs corresponding to these two regions.

3.1. Microstructural observations by TEM

Fig. 1 shows representative TEM images recorded (a) at the center of the disk and (b) near the edge of the disk for pure Cu. Similar images are shown in Figs. 2 and 3 for the Cu–10% Zn and Cu–30% Zn alloys, respectively. Several conclusions may be reached from inspection of these and other similar images.

First, there is a general tendency in each material for smaller grains to form near the peripheries of the disks but with significantly larger grains near the centers. This observation is reasonable because the equivalent von Mises strain, ε_{Eq}, in HPT is given by [32]

$$\varepsilon_{eq} = \frac{2\pi NR}{h\sqrt{3}} \quad (1)$$

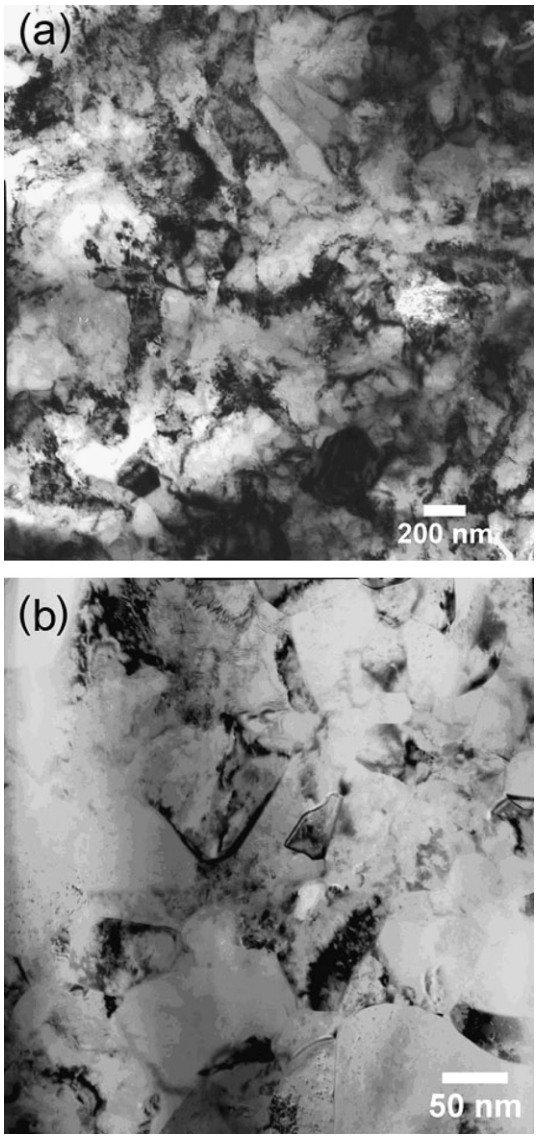

Fig. 1. Images recorded by TEM (a) at the center and (b) near the edge of a disk of pure Cu processed by HPT.

where N is the number of revolutions and h is the height of the disk. Thus, neglecting the pressure imposed on the disk prior to and during the straining operation, the strain arising only from the torsional revolutions is zero at the center of the disk. In practice, however, the presence of a high external applied pressure throughout HPT leads to a straining in the center of each disk, and it was demonstrated earlier that the precise microstructural characteristics in the centers of HPT disks depend upon the rate of recovery in the material and therefore upon the magnitude of the stacking-fault energy [31]. For the three materials tested in the present investigation, the stacking-fault energies are low, the dislocations are widely dissociated, cross-slip is difficult and accordingly the recovery process is very slow.

Second, the grain boundaries appear to be sharper and less wavy near the edges of each disk thereby suggesting

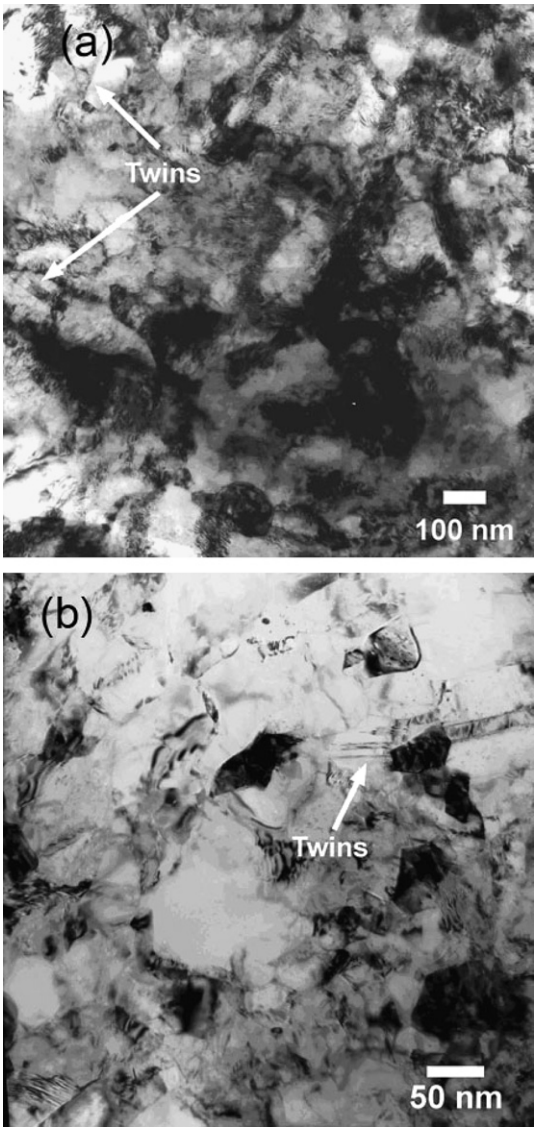

Fig. 2. Images recorded by TEM (a) at the center and (b) near the edge of a disk of Cu–10% Zn processed by HPT.

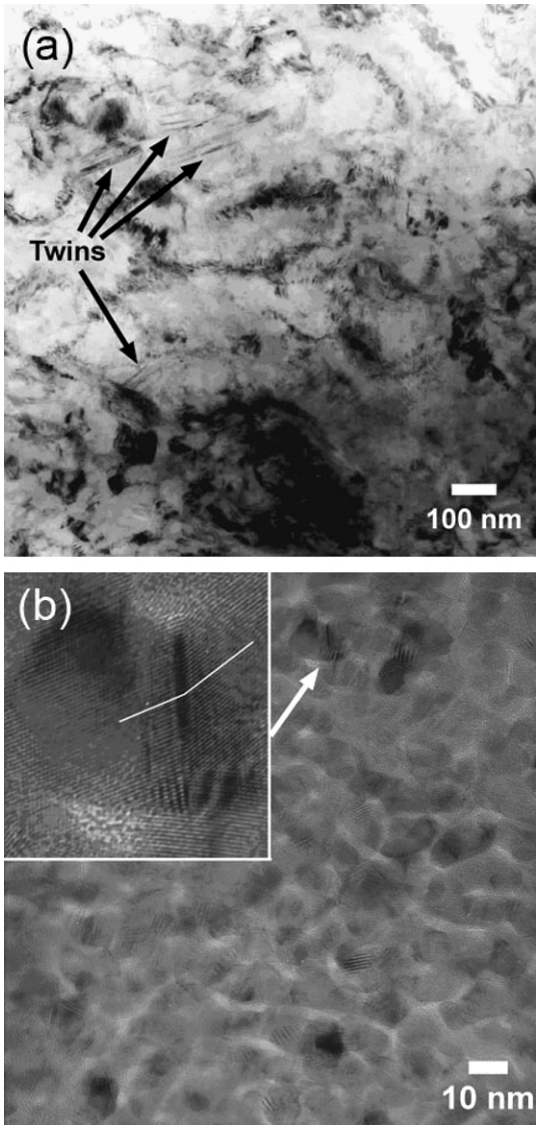

Fig. 3. Images recorded by TEM (a) at the center and (b) near the edge of a disk of Cu–30% Zn processed by HPT.

more equilibrated microstructures in these regions. This observation is reasonable because of the higher strain and greater recovery near the edges of the disks.

Third, extensive observations revealed only a very small number of twins in the pure Cu either at the edge or in the center of the disk, whereas for the Cu–10% Zn alloy twins were easily visible near the edge of the disk but there was only very limited twinning in the central region and there was twinning throughout the disk for the Cu–30% Zn alloy with a very high density of twins near the disk edge.

The individual measurements of the grain sizes in the center regions of the disks, as determined from TEM micrographs, are presented as histograms in Fig. 4 for (a) pure Cu, (b) the Cu–10% Zn alloy and (c) the Cu–30% Zn alloy, respectively. Corresponding histograms were reported earlier [25] for the region of maximum strain near the edges of the disks and the average grain sizes were determined as ~75, ~50 and ~10 nm in the edge regions for these three materials. By contrast, it is evident from Fig. 4 that the grain sizes in the centers of the disks, determined from TEM micrographs, are ~345 nm in pure Cu, ~240 nm in the Cu–10% Zn alloy and ~160 nm in the Cu–30% Zn alloy. For pure Cu and the Cu–10% Zn alloy, the size variation between the edge and the center of the disk is a factor of ~5, whereas this variation is larger, by a factor of ~16, in the Cu–30% Zn alloy. This difference suggests the measured grain size at the edge of the disk in the Cu–30% Zn alloy may be erroneously low due possibly to an overlapping of individual grains within the foils examined by TEM.

An overall conclusion from the TEM observations is that the grains in these materials are extremely small, being <100 nm near the edges of the disks and larger, but within the submicrometer range, in the disk centers.

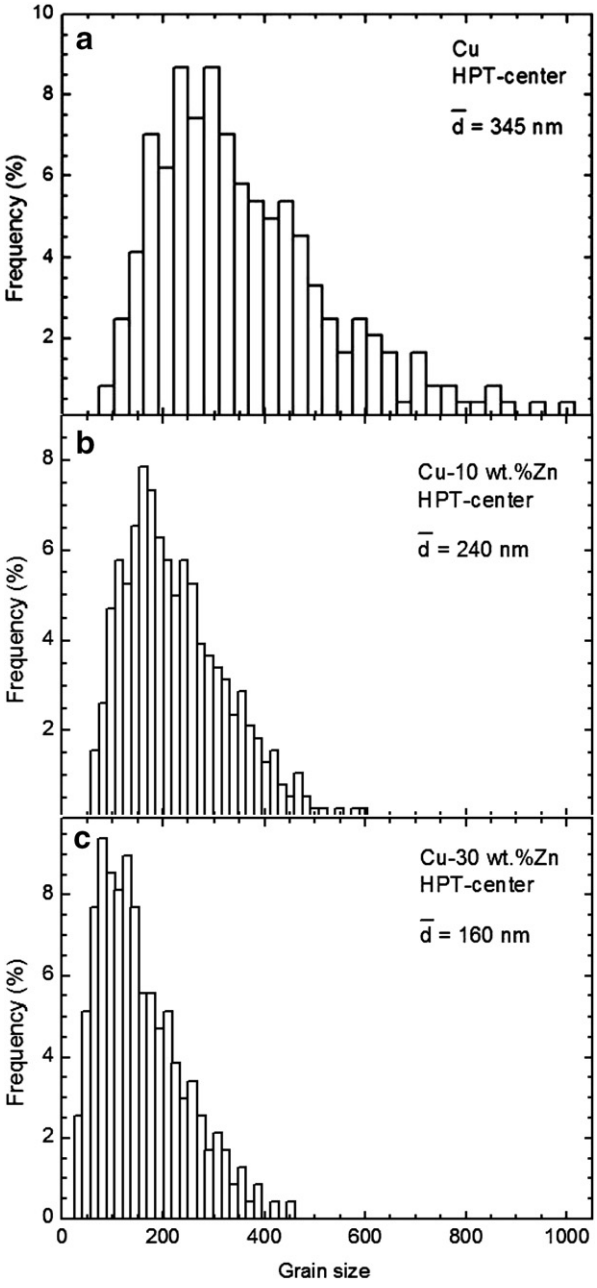

Fig. 4. Histograms showing the grain size distributions at the centers of disks processed by HPT for (a) pure Cu, (b) Cu–10% Zn and (c) Cu–30% Zn.

3.2. Microstructural observations by X-ray diffraction

Special techniques are needed in order to obtain meaningful microstructural information when using X-ray diffraction.

It was shown earlier for XRD that if the Miller indices $(h+k+l)=3m$, where m is an integer, the planar defects do not influence the diffraction sub-profiles, whereas when $(h+k+l)\neq 3m$ the diffraction sub-profiles broaden and/or are shifted [28]. In addition, the profile functions of the affected sub-profiles are essentially Lorentz-type functions, and the breadths and shifts of the different sub-profile types are given by fifth-order polynomials as a function of the densities of the three different species of planar faults. The parameters of these polynomials were compiled into parameter files for use as input data in the eCMWP procedure and the theoretical profile functions, $I^{\mathrm{TH}}_{hkl}(K)$, were then convoluted with the measured instrumental pattern, $I^{\mathrm{INST}}(K)$, and fitted to the measured diffraction patterns by a non-linear least-squares algorithm in which

$$K=\frac{2\sin\theta}{\lambda} \tag{2}$$

where θ is the Bragg angle and λ is the X-ray wavelength [33,34]. The $I^{\mathrm{TH}}_{hkl}(K)$ function is the convolution of the size–strain profile functions, $I^{\mathrm{SS}}_{hkl}(K)$, and the profile functions corresponding to the planar faults, $I^{\mathrm{PF}}_{hkl}(K)$, so that [28]

$$I^{\mathrm{TH}}_{hkl}(K)=I^{\mathrm{SS}}_{hkl}(K)\times I^{\mathrm{PF}}_{hkl}(K) \tag{3}$$

The size–strain profile functions are the convolution of the theoretical size and strain functions assuming both log-normal size distributions and strains caused by the dislocations or by lattice defects having stress fields similar to the dislocations [35]. The profile functions, $I^{\mathrm{PF}}_{hkl}(K)$, are given by [28]

$$I^{\mathrm{PF}}_{hkl}(K)=w_\delta I^{\delta}_{hkl}(K)+\sum_{j=1}^{4} w^j_L I^j_{L,hkl}(K) \tag{4}$$

where I^{δ}_{hkl} is a delta function at the exact Bragg position corresponding to sub-profiles where planar faults do not affect the diffraction profiles so that $(h+k+l)=3n$, $I^j_{L,hkl}$ are the Lorentzian profile functions corresponding to the sub-profiles where the planar faults broaden and/or shift the diffraction profiles so that $(h+k+l)\neq 3n$, and w_δ and w_L are the normalized weight fractions of the multiplicities of the hkl planes corresponding to the sub-profiles unaffected and affected by the planar faults, respectively (here n is an integer).

An earlier report gave both the Williamson–Hall plots of the full widths at half maximum (FWHM) of the profiles recorded at the $(1/2)R$ position for the three different materials and two representative diffraction patterns for the pure Cu and Cu–30% Zn alloy at the $(1/2)R$ position [26]. In the eCMWP procedure, only physically inevitable parameters are used in the non-linear least-squares fitting algorithm. The size distribution is then given by the median and the variance, m and χ, of the log normal size distribution, the dislocation structure is denoted by the average dislocation density, ρ, the arrangement parameter for the effective outer cut-off radius of the dislocations, M, and the strain anisotropy parameter, q, and the planar faults are characterized by densities of either α for the stacking faults or β for the twin boundaries. This approach utilizes a total of six different fitting parameters where two relate to the size distribution, two relate to the dislocation structure and one each relates to the strain anisotropy and the planar faults, respectively.

In this investigation, the planar faults were evaluated by making three consecutive fitting procedures for each of the three different planar fault types, whether intrinsic, extrinsic or twin faults, respectively. The parameter files containing the weights of the sub-profile types and the coefficients of the fifth-order polynomials were obtained separately for the three planar fault types and one was used for each separate running of the eCMWP routine. The type of the prevailing planar fault was then decided by the quality of the fit given by the weighted sum of the squared residuals (WSSR). The reduction of the value of WSSR varied between zero and 20% when the twin density varied from zero (in the case of pure copper) to about 4% (in the case of Cu–30%Zn at the edge of the HPT deformed specimen).

In the present investigation, attempting evaluations by assuming either intrinsic or extrinsic stacking faults provided no reduction in the values of WSSR, and therefore the independent evaluations of dislocation densities and faulting are based on the uncorrelated hkl dependence of the strain anisotropy and faulting, respectively. On the basis of calculations presented elsewhere [28], it can be shown that the ratio of the dislocation contrast factors, C, and the FWHM of the profiles corresponding to twinned crystals, C/μ, vary as 0.82, 1.25, 1.16 and 0.92 for the 111, 220, 420 and 422 reflections, respectively, where μ is the FWHM of the faulted profiles. It is noted that changing the ratio of the edge-screw dislocation character cannot account for the hkl dependence of line broadening caused by twinning or faulting. These ratios are different for different planar defect types, such as intrinsic and extrinsic stacking faults and twin boundaries, and this permits direct identifications of the three defect types. Table 1 summarizes the results from the detailed evaluation and includes the values for m and χ for the log normal size distribution, the area average mean crystallite size, $\langle x\rangle_{\text{area}}$, determined from the relationship [36]

$$\langle x\rangle_{\text{area}} = m\exp(2.5\chi^2) \tag{5}$$

the average dislocation density, ρ, the dislocation arrangement parameter, M, the parameter for strain anisotropy, q, and the average density of twin boundaries, β.

For convenience, Figs. 5–7 plot for the three materials the values of $\langle x\rangle_{\text{area}}$, ρ and β, respectively, against the normalized positions within the disks, where R_0 is the disk radius of 0.5 mm. It is apparent from Fig. 7 that the values estimated for $\langle x\rangle_{\text{area}}$ are similar for pure Cu and Cu–10% Zn, whereas the values estimated for Cu–30% Zn are smaller by a factor of ~2. In addition, the values of $\langle x\rangle_{\text{area}}$ are essentially independent of position for Cu and Cu–30% Zn but they decrease slightly from the center to the edge of the disk for the Cu–10% Zn alloy. For the average dislocation densities shown in Fig. 6, the results tend to be scattered but nevertheless the evidence suggests that ρ is essentially independent of position for pure Cu and the Cu–30% Zn alloy whereas ρ increases from the center to the edge of the disk for the Cu–10% Zn alloy. In addition, the values of ρ are relatively low for Cu and the Cu–10% Zn alloy but are significantly higher for the Cu–30% Zn alloy. The twin densities, β, are shown in Fig. 7, where for pure Cu the measured density is essentially zero throughout the disk but the values of β increase from the centers to the edges of the disks for the two alloys and, in addition, the twin densities are significantly higher in the Cu–30% Zn alloy. Earlier reports have indicated both a small contribution from twinning and an absence of twinning in pure Cu [28,37,38].

3.3. The degree of homogeneity across the disks revealed by hardness measurements

By taking a series of detailed measurements of the Vickers microhardness, H_V, following a rectilinear grid pattern, it is possible to construct maps delineating the variations of local hardness across each disk. Similar approaches were used earlier for pure Al and aluminum alloys processed either by ECAP [39–42] or by HPT [31]. The results obtained in the present investigation are shown in Fig. 8.

Table 1
The median and variance, m and χ, of the log normal size distribution of subgrains, the area average mean crystallite size, $\langle x\rangle_{\text{area}}$, the average dislocation density, ρ, the dislocation arrangement parameter, M, the strain anisotropy parameter, q, and the average density of twin boundaries, β, for the three materials at positions of $0R$, $(1/2)R$ and $1R$, respectively

Position	m (nm)	χ	$\langle x\rangle_{\text{area}}$ (nm)	ρ (10^{14} m^{-2})	M	q	β (%)
Cu							
0 R	51 (5)	0.25 (0.05)	60 (5)	17.5 (3)	1.8 (0.2)	2.38 (0.1)	0.0 (0.02)
(1/2) R	42 (5)	0.38 (0.05)	60 (5)	14.2 (3)	1.8 (0.2)	2.54 (0.1)	0.0 (0.02)
1 R	45 (5)	0.33 (0.05)	59 (5)	19.2 (3)	1.2 (0.2)	2.17 (0.1)	0.0 (0.02)
Cu–10% Zn							
0 R	55 (5)	0.28 (0.05)	67 (5)	9.4 (2)	5 (0.5)	2 (0.1)	0.16 (0.02)
(1/2) R	50 (5)	0.27 (0.05)	60 (5)	34 (5)	2.7 (0.4)	1.85 (0.1)	0.82 (0.02)
1 R	39 (5)	0.33 (0.05)	51 (5)	43 (5)	2.4 (0.4)	2.24 (0.1)	1.36 (0.02)
Cu–30% Zn							
0 R	25 (3)	0.3 (0.05)	31 (3)	97 (7)	4 (0.5)	2.52 (0.1)	1.82 (0.02)
(1/2) R	29 (3)	0.25 (0.05)	34 (3)	81 (7)	4 (0.5)	2.4 (0.1)	2.88 (0.02)
1 R	24 (3)	0.29 (0.05)	30 (3)	117 (10)	3.7 (0.4)	2.6 (0.1)	3.73 (0.02)

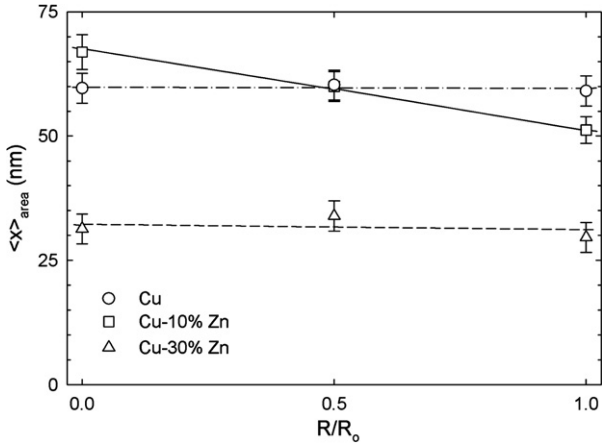

Fig. 5. Measurements by XRD of the area average mean crystallite size across the radius of disks of pure Cu, and Cu–10% Zn and Cu–30% Zn alloys.

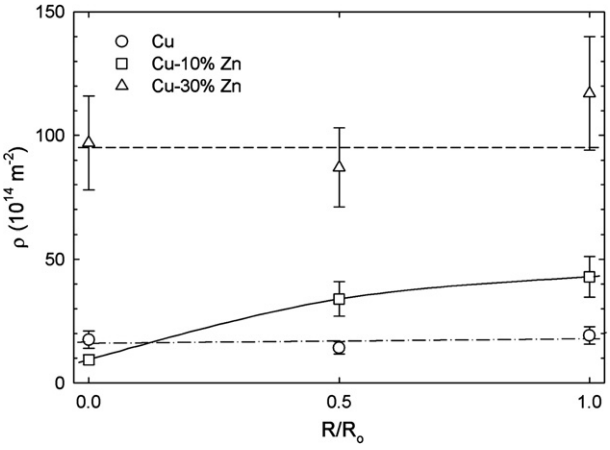

Fig. 6. Measurements by XRD of the average dislocation density across the radius of disks of pure Cu, amd Cu–10% Zn and Cu–30% Zn alloys.

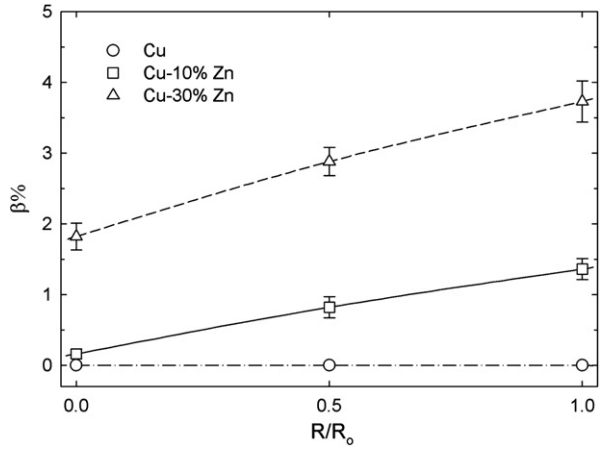

Fig. 7. Measurements by XRD of the average density of twin boundaries across the radius of disks of pure Cu, amd Cu–10% Zn and Cu–30% Zn alloys.

Two conclusions may be reached from these plots. First, there are regions of significantly lower hardness in the vicinities of the centers of the disks for the two Cu–Zn alloys whereas the hardness decreases only to a minor extent for pure Cu in the disk center. The results for the alloys are generally consistent with the grain sizes measured by TEM which are substantially smaller near the edges of the disks. However, the TEM observations also show a significant decrease in grain size in pure Cu in the center of the disk and this is reflected only marginally by the hardness measurements. Second, in terms of the relative values of H_V, the highest hardness is recorded in Cu–30% Zn, there is an intermediate hardness in Cu–10% Zn and the hardness is lowest in pure Cu. These results are consistent with the magnitudes of the grain sizes measured by TEM.

To provide quantitative information on the local values of the Vickers microhardness, Fig. 9 plots the individual values of H_V determined along linear traverses across the three disks for the three different materials. These results were obtained by taking individual values of the microhardness across the diameter of each disk in incremental steps at positions separated by 0.6 mm up to a distance of 1.2 mm on either side of the center of each disk and then at greater distances from the centers the measurements were taken in incremental steps of either 0.6 or 1.2 mm. At each position, the value of the hardness was estimated by averaging the individual measurements recorded at four separate points uniformly positioned around the selected point at a distance of 0.15 mm. The error bars visible in Fig. 9 were calculated at the 95% confidence level for each of these separate positions. Table 2 summarizes the average values of H_V, and the associated error bars at the 95% confidence level, for measurements taken at the selected positions of $0R$, $(1/2)R$ and $1R$. These results show relatively small variations in H_V across the disks for pure Cu and the Cu–30% Zn alloy but there is a very pronounced variation in H_V for the Cu–10% Zn alloy.

4. Discussion

4.1. An overview of the experimental data

The present investigation was conducted on three different materials processed by HPT and using three separate procedures for microstructural observations. The results show both consistencies and apparent inconsistencies between these various sets of data and it is important therefore to examine these apparent differences.

First, for pure Cu the twin density is zero in Fig. 7 and the dislocation densities in Fig. 8 and the grain or subgrain sizes in Fig. 5 are both independent of the position in the disk. Furthermore, there is only a relatively minor change in the measured hardness across the disk of pure Cu, as shown in Figs. 8 and 9. These results are generally in agreement with a recent report documenting the microstructures and strength characteristics of pure Cu processed by HPT

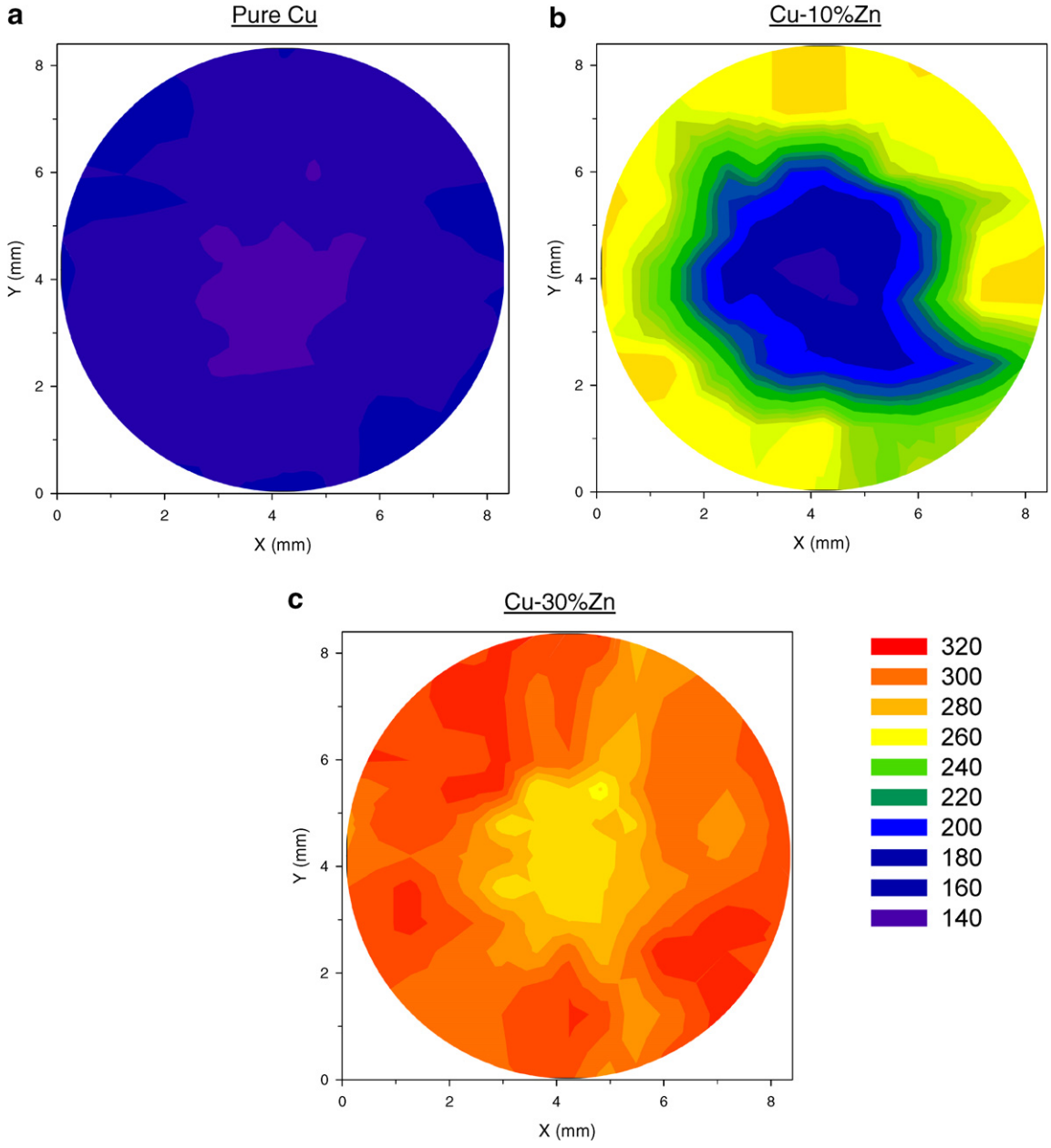

Fig. 8. Color-coded contour maps showing the variation in Vickers microhardness across the surfaces of disks of pure Cu, Cu–10% Zn and Cu–30% Zn processed by HPT; the significance of the colors is shown by the inset on the right.

under a range of applied pressures [43]. By contrast, for the Cu–10% Zn alloy the twin and dislocation densities increase and the grain size decreases from the center to the edge of the disk, in apparent agreement with the microhardness measurements, whereas for the Cu–30% Zn alloy the dislocation density and average grain or subgrain size remain reasonably constant across the disk, the twin density increases towards the periphery but the microhardness measurements reveal an increase in hardness near the edge of the disk. It is reasonable to conclude from these separate observations that the increasing hardness around the periphery of the disk is due primarily to the influence of twinning in the alloy. Furthermore, since β increases towards the edges of the disks in both of the Cu–Zn alloys, as shown in Fig. 7, it is probable that twinning also accounts for some of the very significant change in microhardness revealed in the Cu–10% Zn alloy in Figs. 8 and 9.

An important additional characteristic is shown by the color-coded contour maps in Fig. 8. These plots demonstrate a reduction in hardness near the centers of the disks for the two Cu–Zn alloys and this is supported by the quantitative measurements in Fig. 9. In an earlier similar investigation of pure Al processed by HPT, it was shown that the hardness values were higher, rather than lower, in the centers of the disks at low imposed strains [31]. Furthermore, by making use of earlier hardness measurements on an Al-6061 alloy processed by ECAP [40], it

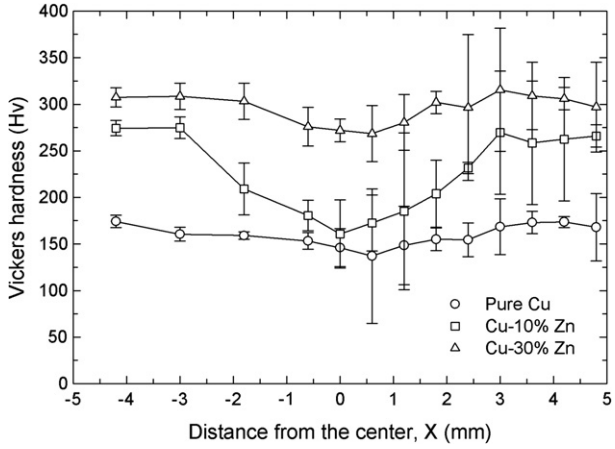

Fig. 9. Variation in the Vickers microhardness across diameters of disks of pure Cu, Cu–10% Zn and Cu–30% Zn processed by HPT.

Table 2
Average values of H_V at the three positions on the HPT disk used for XRD

Material	Position on HPT disk		
	0	(1/2) R	1 R
Cu	145 ± 15	155 ± 3	168 ± 5
Cu–10% Zn	158 ± 26	232 ± 2	266 ± 2
Cu–30% Zn	272 ± 2	296 ± 12	298 ± 8

was suggested that, relative to the values of hardness at the disk edges, the values of H_V in the disk centers may increase for materials exhibiting fast recovery rates but decrease for materials exhibiting slow recovery rates. The present results are fully consistent with this proposal because the very low stacking-fault energies in the Cu–Zn alloys lead to slow rates of recovery.

4.2. A quantitative correlation between the microstructural parameters and the flow mechanism

It is well established that the applied stress, σ, the average grain size, $\langle x\rangle_{area}$, and the average dislocation density, ρ, may be correlated using either the Hall–Petch or the Taylor relationship. The Hall–Petch equation relates the flow stress, σ, to the grain size, d, according to [44,45]

$$\sigma = \sigma_0 + K^{HP} d^{-1/2} \tag{6}$$

where σ_0 is the friction stress and K^{HP} is the Hall–Petch constant. Alternatively, in the modified Taylor relationship the shear stress, τ, is related to the dislocation density, ρ, by [46–48]

$$\tau = \tau_0 + \alpha G \mathbf{b} \rho^{1/2} \tag{7}$$

where τ_0 is the critical resolved shear stress, α is a constant lying between zero and unity, G is the shear modulus and $\mathbf{b}$ is the Burgers vector. In order to correlate the measured hardness values with the dislocation densities, Eq. (7) may be rewritten in terms of the applied stress so that

$$\sigma = \sigma_0 + M^T \alpha G \mathbf{b} \rho^{1/2} \tag{8}$$

where M^T is the Taylor factor.

Table 3 summarizes the constants used in Eqs. (6)–(8) for the three different materials, including the values of G [49] and the values of K^{HP} and σ_0 [50–52]. To determine the precise significance of Eqs. (6) and (8) in the present investigation, it is necessary to use the values summarized for H_V in Table 2 at the three points within the disk where the X-ray diffraction data were recorded. Using Eq. (6) and with $M^T = 3$ and $\alpha = 0.3$ in Eq. (8), Fig. 10 shows the values calculated for σ from the Hall–Petch and Taylor relationships plotted against the individual values of σ derived from the measurements of H_V by taking $\sigma \approx H_V/3$ [53], where the error bars were calculated from the error estimates of the dislocation density and the grain size evaluations, respectively. It is apparent from this plot that the Hall–Petch relationship tends to overestimate the stress whereas the Taylor relationship gives values for the stress which are reasonably consistent with the measured values.

The failure to obtain consistency with the Hall–Petch relationship is unexpected because earlier studies demonstrated excellent agreement with this relationship when using microhardness measurements taken on various aluminum-based alloys processed by ECAP [53–55]. Accordingly, it is necessary to examine the reason for this inconsistency.

It is reasonable to anticipate the discrepancy arises when using Eq. (6) because of the different procedures used to determine the average grain size. In Table 3, the values of the constant, K^{HP}, were estimated from average grain sizes measured using either optical microscopy [51,52] or TEM [49,51]. By contrast, the present calculations make use of the average mean crystallite size, $\langle x\rangle_{area}$, determined from X-ray line broadening. The correlation between the TEM and the X-ray crystallite sizes was examined recently [56] and it was shown that, especially in heavily deformed bulk metals, the X-ray crystallite size is essentially identical to, or at least very close to, the subgrain size. Thus, the coherency of X-ray scattering is broken by the dislocation cell

Table 3
Values used in evaluating the Hall–Petch and Taylor relationships

Material	G (GPa)	K^{HP} (MPa m$^{1/2}$)	$\mathbf{b}$ (nm)	σ_0 (MPa)	K^{HP}_{SG} (MPa m$^{1/2}$)	N_{SG}
Cu	47.7 [49]	0.15 [50,51]	0.255	23	0.125	2
Cu–10% Zn	45.5 [49]	0.20	0.255	30	0.166	2
Cu–30% Zn	41.0 [49]	0.29 [51,52]	0.256	44 [51,52]	0.166	9

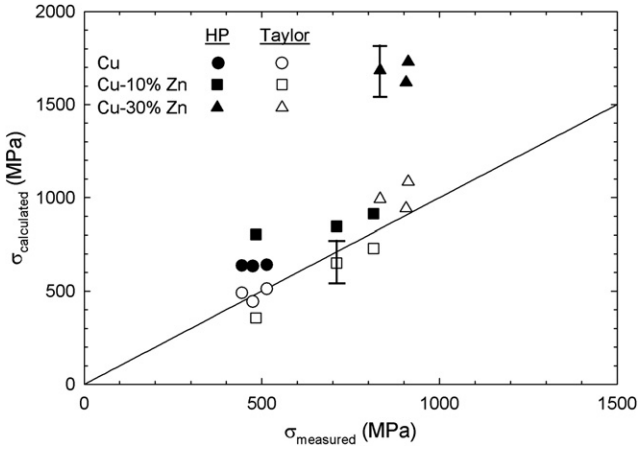

Fig. 10. A comparison of the values of stress calculated from the Hall–Petch and Taylor relationships against the values of stress derived directly from the hardness measurements; two representative error bars are shown based on the error estimates incorporated into the evaluations of the dislocation density and grain size, respectively.

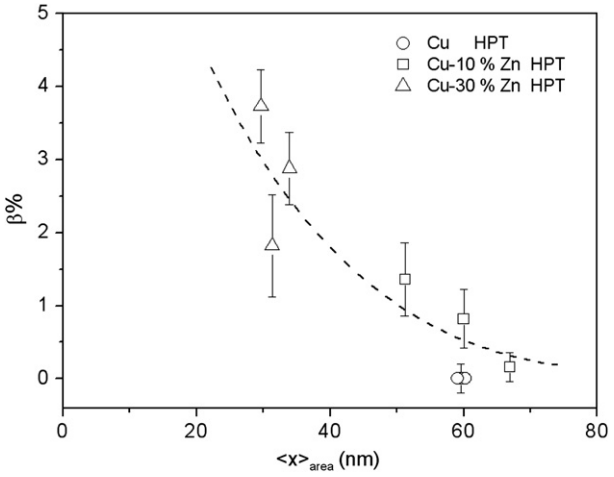

Fig. 11. The twin density plotted against the mean crystallite size showing the occurrence of twinning at crystallite sizes less than ~60 nm; the error bars are calculated from error estimates incorporated in the twin density evaluations.

walls, which may be arranged either as low-angle grain boundaries or as dipolar-wall configurations. Since these are the two extremes of dislocation cell wall configurations, any real dislocation cell wall boundaries will also break the coherency of X-ray scattering, which means in practice that the measured X-ray crystallite sizes, especially in bulk metals, represent dislocation cells or subgrain sizes that are generally smaller than the grain sizes determined by conventional TEM. The use of these smaller subgrain sizes will lead to an overestimation of σ, as shown in Fig. 10.

Using the present values of $\langle x\rangle_{\text{area}}$, calculations were made to determine the appropriate values for the Hall–Petch constant, $K_{\text{SG}}^{\text{HP}}$, associated with the average subgrain size, and these values are also listed in Table 3. From this approach, the Hall–Petch relationship in Eq. (6) may be expressed independently for grains and subgrains in the form

$$\sigma - \sigma_0 = K^{\text{HP}} d_G^{-1/2} = K_{\text{SG}}^{\text{HP}} d_{\text{SG}}^{-1/2} \tag{9}$$

where d_{G} and d_{SG} are the average grain and subgrain sizes, respectively. Making the reasonable assumption that the values of d_{G} are readily measured by TEM or optical microscopy whereas d_{SG} relates to the values measured by X-ray line profile analysis, the area average mean number of subgrains per grain, N_{SG}, is given by

$$N_{\text{SG}} = \left(\frac{d_{\text{G}}}{d_{\text{SG}}}\right)^2 = \left(\frac{K_{\text{G}}}{K_{\text{SG}}}\right)^4 \tag{10}$$

The values estimated for N_{SG} are given in the last column of Table 3 and they show that $N_{\text{SG}} \approx 2$ for pure Cu and the Cu–10% Zn alloy whereas $N_{\text{SG}} \approx 9$ for the Cu–30% Zn alloy where there is the greatest discrepancy between measurements and calculations as shown in Fig. 10. For Cu and Cu–10% Zn, reference to Table 1 shows that the dislocation densities are not large, varying between $\sim 1 \times 10^{15}$ and $\sim 4 \times 10^{15}\,\text{m}^{-2}$, whereas for Cu–30% Zn the measured dislocation densities are higher and close to $\sim 1 \times 10^{16}\,\text{m}^{-2}$.

4.3. The significance of twinning

The role of twinning may be compared qualitatively by examining the variations along the disk radii of the hardness measurements and the dislocation and twin density distributions for the two alloys containing Zn; these plots are shown in Figs. 6, 7 and 9. In the Cu–10% Zn alloy, both the twin density and the dislocation density increase with increasing distance from the center of the disks and there is an unusually large increase in the values of H_{V} over the same length. By contrast, in the Cu–30% Zn alloy the twin density increases significantly, the dislocation density remains reasonably constant and the values of H_{V} increase to only a relatively minor extent. In practice, however, these two sets of data are mutually consistent and demonstrate that the increase in hardness in the Cu–10% Zn alloy is due to contributions from both the twins and the dislocations whereas in the Cu–30% Zn alloy the increase is due almost exclusively to twinning.

The significance of twinning in these materials is illustrated in Fig. 11. where the twin density, β, is plotted against the mean crystallite size, $\langle x\rangle_{\text{area}}$, and the error bar was calculated from an error estimation for the twin density evaluation. It is concluded from this plot that twinning becomes significant only when the crystallite size is less than ~60 nm. This is consistent with an earlier study suggesting that twinning in pure Cu requires a crystallite size of less than ~40–50 nm [28,38].

5. Summary and conclusions

1. Disks of pure Cu, a Cu–10% Zn alloy and a Cu–30% Zn alloy were processed by high-pressure torsion through

five revolutions under an imposed pressure of 6 GPa. These materials were selected because they have very low stacking-fault energies of ~41, ~22 and ~7 mJ m^{-2}, respectively. Following torsional straining, the disks were examined by transmission electron microscopy and X-ray diffraction, and by taking measurements of the Vickers microhardness.

2. All three materials showed a variation in microstructure across the disks, with larger grains occurring in the grain centers. At the peripheries of the disks the grain sizes measured by TEM were ~75, ~50 and ~10 nm for pure Cu, Cu–10% Zn and Cu–30% Zn, respectively, whereas in the centers of the disks the average grain sizes were in the lower submicrometer range. Smaller crystallite sizes were measured in the disk centers using X-ray diffraction.
3. Measurements were taken by XRD at three selected positions on each disk to determine the dislocation and twinning densities. These measurements showed essentially an absence of twinning in pure Cu but increases in both the dislocation density and the twin density with increasing Zn content and therefore with decreasing stacking-fault energy.
4. Detailed measurements of the Vickers microhardness revealed lower hardness values in the disk centers for the two Cu–Zn alloys. This result supports an earlier suggestion that the values of hardness will be lower in the disk centers when using materials having slow recovery rates.

Acknowledgements

This work was supported in part by the Hungarian National Science Foundation under Grant Nos. OTKA T46990 and OTKA T43247 (T.U. and L.B.), in part by the IPP program of the US Department of Energy (Y.T.Z.), in part by a Grant-in-Aid for Scientific Research from the Ministry of Education, Culture, Sports, Science and Technology of Japan on Priority Area "Giant Straining Process for Advanced Materials Containing Ultra-High Density Lattice Defects" (Z.H.) and in part by the National Science Foundation of the United States under Grant No. DMR-0243331 (C.X. and T.G.L.).

References

[1] Valiev RZ, Islamgaliev RK, Alexandrov IV. Prog Mater Sci 2000;45:103.
[2] Valiev RZ, Langdon TG. Prog Mater Sci 2006;51:881.
[3] Horita Z, Fujinami T, Langdon TG. Mater Sci Eng 2001;A318:324.
[4] Huang Y, Prangnell PB. Scripta Mater 2007;56:333.
[5] Chen Z-H, Cheng Y-Q, Xia W-J. Mater Manufact Process 2007;22:51.
[6] Raab GJ, Valiev RZ, Lowe TC, Zhu YT. Mater Sci Eng 2004;A382:30.
[7] Zhilyaev AP, Nurislamova GV, Kim B-K, Barö MD, Szpunar JA, Langdon TG. Acta Mater 2003;51:753.
[8] Zehetbauer MJ, Stüwe HP, Vorhauer A, Schafler E, Kohout J. In: Zehetbauer MJ, Valiev RZ, editors. Nanomaterials by Severe Plastic Deformation. Weinheim: Wiley-VCH; 2004. p. 435.
[9] Valiev RZ, Estrin Y, Horita Z, Langdon TG, Zehetbauer MJ, Zhu YT. JOM 2006;58(4):33.
[10] Bridgman PW. Studies in large plastic flow and fracture. New York: McGraw-Hill; 1952.
[11] Sakai G, Nakamura K, Horita Z, Langdon TG. Mater Sci Eng 2005;A406:268.
[12] Stolyarov VV, Zhu YT, Lowe TC, Islamgaliev RK, Valiev RZ. Nanostruct Mater 1999;11:947.
[13] Jiang H, Zhu YT, Butt DP, Alexandrov IV, Lowe TC. Mater Sci Eng 2000;A290:128.
[14] Zhilyaev AP, Kim B-K, Nurislamova GV, Barö MD, Szpunar JA, Langdon TG. Scripta Mater 2002;48:575.
[15] Zhilyaev AP, Kim B-K, Szpunar JA, Barö MD, Langdon TG. Mater Sci Eng 2005;A391:377.
[16] Dutkiewicz J, Kuśnierz J, Maziarz W, Lejkowska M, Garbacz H, Lewandowska M, et al. Phys Status Solidi (a) 2005;202:2309.
[17] Zhao YH, Zhu YT, Liao XZ, Horita Z, Langdon TG. Mater Sci Eng 2007;A463:22.
[18] Zhu YT, Liao XZ, Srinivasan SG, Lavernia EJ. J Appl Phys 2005;98:034319.
[19] Zhu YT, Liao XZ, Valiev RZ. Appl Phys Lett 2005;86:103112.
[20] Čížek J, Procházka I, Melikhova O, Brauer I, Anwand W, Kužel R, et al. Appl Surf Sci 2002;194:140.
[21] Čížek J, Procházka I, Brauer G, Anwand W, Kužel R, Cieslar M, et al. Phys Status Solidi (a) 2003;195:335.
[22] Révész Á, Hóbor S, Lábár JL, Zhilyaev AP, Kovács Zs. J Appl Phys 2006;100:103522.
[23] Kovács Zs, Hóbor S, Szabo PJ, Lendvai J, Zhilyaev AP, Révész Á. Mater Sci Eng 2007;A449–451:1139.
[24] Carter CB, Ray ILF. Phil Mag 1977;35:189.
[25] Zhao YH, Liao XZ, Zhu YT, Horita Z, Langdon TG. Mater Sci Eng 2005;A410–411:188.
[26] Ungár T, Balogh L, Zhu YT, Horita Z, Xu C, Langdon TG. Mater Sci Eng 2007;A444:153.
[27] Sakai G, Horita Z, Langdon TG. Mater Sci Eng 2005;A393:344.
[28] Balogh L, Ribárik G, Ungár T. J Appl Phys 2006;100:023512.
[29] Treacy MJ, Newman JM, Deem MW. Proc Roy Soc Lond A 1991;433:499.
[30] Ribárik G, Gubicza J, Ungár T. Mater Sci Eng 2004;A387–389:343.
[31] Xu C, Horita Z, Langdon TG. Acta Mater 2007;55:203.
[32] Wetscher F, Vorhauer A, Stock R, Pippan R. Mater Sci Eng 2004;A387–389:809.
[33] Ribárik G, Ungár T, Gubicza J. J Appl Cryst 2001;34:669.
[34] Ribárik G, Gubicza J, Ungár T. Mater Sci Eng 2004;A387–389:343.
[35] Ungár T, Gubicza J, Ribárik G, Borbély A. J Appl Cryst 2001;34:298.
[36] Hinds WC. Aerosol technology: properties, behavior and measurement of airborne particles. New York: Wiley; 1982.
[37] Liao XZ, Zhou F, Lavernia EJ, He DW, Zhu YT. Appl Phys Lett 2003;83:5062.
[38] Liao XZ, Zhao YH, Zhu YT, Valiev RZ, Gunderov DV. J Appl Phys 2004;96:636.
[39] Xu C, Langdon TG. Scripta Mater 2003;48:1.
[40] Xu C, Furukawa M, Horita Z, Langdon TG. Mater Sci Eng 2005;A398:66.
[41] Xu C, Xia K, Langdon TG. Acta Mater 2007;55:2351.
[42] Xu C, Langdon TG. J Mater Sci 2007;42:1542.
[43] Schafler E, Dubravina A, Mingler B, Karnthaler HP, Zehetbauer M. Mater. Sci Forum 2006;503–504:51.
[44] Hall EO. Proc Phys Soc B 1951;64:747.
[45] Petch NJ. J Iron Steel Inst 1953;174:25.
[46] Taylor GI. Proc Roy Soc Lond A 1934;145:362.
[47] Wiedersich H. J Metals 1964;16:425.
[48] Kassner ME. Acta Mater 2004;52:1.
[49] Jiang Z, Lian J, Baudelet B. Acta Metall Mater 1995;43:3349.

[50] Hansen N, Ralph B. Acta Metall 1982;30:411.
[51] Nagarjuna S, Srinivas M, Sharma KK. Acta Mater 2000;48:1807.
[52] Meakin JD, Petch NJ. Phil Mag 1974;29:1149.
[53] Furukawa M, Horita Z, Nemoto M, Valiev RZ, Langdon TG. Phil Mag 1998;78:203.
[54] Furukawa M, Horita Z, Nemoto M, Valiev RZ, Langdon TG. Acta Mater 1996;44:4619.
[55] Furukawa M, Iwahashi Y, Horita Z, Nemoto M, Tsenev NK, Valiev RZ, et al. Acta Mater 1997;45:4751.
[56] Ungár T, Tichy G, Gubicza J, Hellmig R. Powder Diffr 2005;20:366.